SHIFT-TOLERANT PERCEPTUAL SIMILARITY METRIC

Anonymous authors
Paper under double-blind review

ABSTRACT

Existing perceptual similarity metrics assume an image and its reference are well aligned. As a result, these metrics are often sensitive to a small alignment error that is imperceptible to the human eyes. This paper studies the effect of small misalignment, specifically a small shift between the input and reference image, on existing metrics, and accordingly develops a shift-tolerant similarity metric. This paper builds upon LPIPS, a widely used learned perceptual similarity metric and explores architectural design considerations to make it robust against imperceptible misalignment. Specifically, we study a wide spectrum of neural network elements, such as anti-aliasing filtering, pooling, striding, padding, and skip connection, and discuss their roles in making a robust metric. Based on our studies, we develop a new deep neural network-based perceptual similarity metric. Our experiments show that our metric is tolerant to imperceptible shifts while being consistent with the human similarity judgment.

1 INTRODUCTION

Image similarity measurement is a common task for many computer vision and computer graphics applications. General similarity metrics like PSNR and RMSE, however, do not match the human visual perception well when assessing the similarity between two images. Therefore, many dedicated image similarity metrics, such as Structural Similarity (SSIM) and its variations (Wang et al., 2004; 2003; Zhang et al., 2011), were developed in order to more closely reflect the human perception. However, manually crafting a perceptual similarity metric remains a challenging task as it involves the complex human cognitive judgement (Medin et al., 1993; Tversky, 1977; Wang et al., 2004; Zhang et al., 2018).

Recently, learning-based image similarity metrics have been developed. These metrics learn from a large set of labelled data and are able to predict the similarity between two images that correlates well with the human perception (Bhardwaj et al., 2020; Ding et al., 2020; Kettunen et al., 2019; Prashnani et al., 2018; Zhang et al., 2018; Czolbe et al., 2020). Among them, the Learned Perceptual Image Patch Similarity metric (LPIPS) by Zhang et al. (2018) is now widely adopted as a perceptual image similarity metric and used in computer graphics and vision literature.

This paper studies how image similarity metrics work on a pair of images that are not perfectly aligned. For instance, a tiny misalignment in the image pair such as a one-pixel translation between them, is imperceptible to the human eyes. But, *will such a visually imperceptible misalignment compromise any existing similarity metrics*? For PSNR and RMSE, since they assume pixel-wise registration, naturally they are sensitive to as small as a one-pixel misalignment. As we will detail in this paper, our study found that the learned perceptual similarity metrics, such as LPIPS, are also sensitive to a small misalignment. Figure 1 shows such an example through a two-alternative forced choice test. In this test, viewers were asked "*which of the two distorted images, I_0 or I_1,*

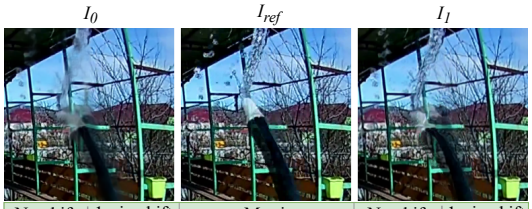

No-shift	1-pix-shift	Metric	No-shift	1-pix-shift
		Humans	✓	✓
✓		MS-SSIM		✓
✓		L2		✓
✓		LPIPS (Alex)		✓

Figure 1: Whether two images I_0 and I_1 are shifted by 1 pixel or not, viewers always consider I_1 is more similar to I_{ref} than I_0. However, existing metrics often switch their predictions after the imperceptible 1-pixel shift.

is more similar to the reference image I_{ref}?" Then, we shifted I_0 and I_1 by one pixel and obtained their opinions again. None of the participants flipped their opinions from I_0 to I_1 or vice versa, which is intuitive as a one-pixel shift is imperceptible to viewers. But existing metrics, such as MS-SSIM and LPIPS, flipped their judgments after the one-pixel shift.

Our problem is related to the recent work on making deep neural networks shift invariant (Islam et al., 2020; Kayhan & Gemert, 2020; Vasconcelos et al., 2021; Zhang, 2019; Zou et al., 2020; Lee et al., 2020). In a recent study, Azulay & Weiss (2019) found that an image classifier can change its top-1 prediction if the image is translated by only one pixel. Their results showed that after translating an image by one pixel, the classifier made a different top-1 prediction for 30% of the 1000 validation images. Zhang (2019) introduced anti-aliasing filters into a deep neural network to make the feature extraction network shift-equivariant, which in term makes the whole network shift-invariant for the down streaming tasks. Compared to these works, our problem is different in that 1) a perceptual similarity metric takes two images as input instead of working on a single input image, and 2) only one of the two images is shifted, thus introducing imperceptible misalignment instead of shifting the two images simultaneously.

This paper aims to develop a shift-tolerant perceptual similarity metric that correlates well with the human judgement on the similarity between images while being robust against imperceptible misalignment between them. We build our metric upon LPIPS, a deep neural network-based metric that is now widely adopted for its close correlation with the human perception. We investigate a variety of elements that can be incorporated into a deep neural network to make it resistant to an imperceptible misalignment. These elements include anti-aliasing filters, striding, pooling, padding, placement of anti aliasing, etc. Based on our findings on these elements, we develop a shift-tolerant perceptual similarity metric that not only is more consistent with human perception but also is significantly more resistant to imperceptible misalignment between a pair of images than existing metrics.

In the remainder of this paper, we first report our study that verifies that viewers are not sensitive to small amount of shifts between two images when comparing them, in Section 3. We then benchmark existing visual similarity metrics and show that these metrics are sensitive to imperceptible shifts between a pair of images in Section 4. We then study several important elements that make a deep neural network-based similarity metric both tolerant to imperceptible shifts and consistent with the human perception of visual similarity in Section 5. We finally report our experiments that thoroughly evaluate our new perceptual similarity metric by comparing it to state of the art metrics and through detailed ablation studies in Section 6.

2 Related Work

Visual similarity metrics are commonly used to compare two images or evaluate the performance of many image and video processing, editing and synthesis algorithms. While there are already many established metrics for these tasks, such as PSNR, MSE, SSIM and its variations (Wang et al., 2004; 2003), there is still a gap between their prediction and the human's judgement. This section provides a brief overview of the recent advances in learned perceptual similarity metrics that aim to bridge the gap mentioned above.

In their influential work, Zhang et al. (2018) reported that features from a deep neural network can be used to measure the similarity between two images that is more consistent with the human perception than other commonly used metrics. Accordingly, they developed LPIPS, a perceptual metric learned from a large collection of labelled data. Specifically, LPIPS uses a pre-trained network for image classification tasks or learns a neural network to compute the features for each of the two images or patches, and also learns to aggregate the feature distances into a similarity score. Since its debut, LPIPS has been widely used as a perceptual quality metric. On a related note, the computer vision and graphics community also calculate the difference between the deep features of two images as a loss function to train deep neural networks for image enhancement and synthesis. Such a loss function, often called perceptual loss, enables the neural networks to learn to generate perceptually pleasing images (Dosovitskiy & Brox, 2016; Johnson et al., 2016; Ledig et al., 2016; Niklaus et al., 2017; Sajjadi et al., 2016; Zhu et al., 2016).

Kettunen et al. (2019) developed the E-LPIPS metric that adopts the LPIPS network and uses randomly transformed samples to calculate expected LPIPS distance over them. They showed that E-

LPIPS is robust against the Expectation Over Transformation attack (Athalye et al., 2018). Different from LPIPS, Prashnani et al. (2018) use the differences between features to generate patch-wise errors and corresponding weights, via two different fully-connected networks. Their final similarity score is a weighted average of the patch-wise distances. Czolbe et al. (2020) developed a similarity metric based on Watson's perceptual model (Watson, 1993), by replacing discrete cosine transform with discrete fourier transform (DFT). They posit that their metric is robust against small translations and is sensitive to large translations. Czolbe et al. (2020) used Watson-DFT as a differentiable loss function for image generation via variational autoencoders (Kingma & Welling, 2013).

In their work on image quality assessment, Ma et al. (2018) developed a geometric transformation invariant method (GTI-CNN). Our work is closely related to theirs, as GTI-CNN is a similarity metric that is invariant to the misalignment between a pair of images. In their method, Ma et al. (2018) train a fully convolutional neural network to extract deep features from each image and calculate the mean squared error between them as their final similarity. They showed that training the fully convolutional neural network directly on aligned samples leads to a metric that is sensitive to the misalignment, which is consistent with what we found in our study. They reported that augmenting the training samples with small misalignment can make the learned metric significantly more resistant to the misalignment. Compared to this method, our work focuses on designing a deep neural network architecture that is robust to misalignment without any data augmentation. Bhardwaj et al. (2020) followed the understanding of the physiology of the human visual system and developed a fully convolutional neural network that generates a multi-scale probabilistic representation of an input image and then calculates the symmetric Kullback–Leibler divergences between such representations of two images to measure their similarity. They found that such a similarity metric is robust against small shifts between a pair of images. While benchmarking existing metrics, our study also finds that their metric is most robust against small shifts among all the metrics we tested. We posit that the robustness of their method partially comes from training their metric on neighboring video frames that might already have small shifts among them, thus effectively serving as data augmentation, as done by Ma et al. (2018). We consider these as orthogonal efforts in developing a robust similarity metric. Also, as shown in our study, our metric is more consistent with the human judgement and more robust against imperceptible misalignment than these methods, even though our metric is trained on aligned samples directly without any data augmentation.

Our work is most related to deep image structure and texture similarity (DISTS) metric by Ding et al. (2020). They replaced the max pooling layers with l_2 pooling layers (Hénaff & Simoncelli, 2016) in their VGG backbone network for anti-aliasing. Ding et al. (2020) also found that blurring the input with l_2 pooling makes their network more robust against small shifts. Gu et al. (2020) found that existing metrics like LPIPS do not perform well with images generated by GAN-based restoration algorithms. They attributed it to the small misalignment between the GAN results and the ground truth. Therefore, they used l_2 pooling (Ding et al., 2020; Hénaff & Simoncelli, 2016) and *BlurPool* (Zhang, 2019) to improve LPIPS. They found that both can improve LPIPS while *BlurPool* performs better. Compared to these two recent papers, our paper systematically investigates a broad range of neural network elements besides *BlurPool*. By integrating these elements together, we develop a perceptual similarity metric that is both robust against small shifts and is consistent with the human visual similarity judgement. Our method outperforms existing metrics, and a variety of recently developed learned metrics. Integrating multiple network elements together makes our metric better than individual ones, including *BlurPool*.

3 HUMAN PERCEPTION OF SMALL SHIFTS

As commonly expected, shifting one image by a few pixels will not alter human similarity judgement on a pair of images (Bhardwaj et al., 2020; Xiao et al., 2018). We conducted a user study to verify this common belief. Our hypothesis is that *it is difficult for people to detect a small shift in images*.

In our study, we randomly picked 50 images from the MS-COCO test dataset (Lin et al., 2014). For each participant, we randomly divided these 50 images into 10 groups, each with 5 images. For each image in Group n with $n \in [0, 10)$, we cropped a 256×256 patch as a reference image and shifted the cropping window by n pixels to produce its shifted version. In this way, we generated 50 pairs of images for each participant. During the study, each participant was presented a pair of images one at a time. The order of the 50 pairs of images is also randomized for each participant.

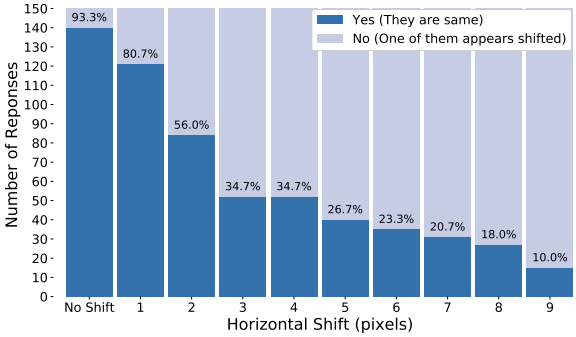

Figure 2: Human perception of small shifts. Image pairs with 1- and 2-pixel shift are deemed the same in 80.7% and 56.0% of the responses, respectively.

In each trial, a pair of images were placed side by side. The position of the reference image, e.g. right or left, is randomized to avoid any bias. We asked our participants to judge whether a pair of images are the same or not. We refer the reader to Appendix A.1 for more details on our study's methodology.

We report the user responses in Figure 2. When the amount of shift is small, participants find it difficult to detect the shift. For pairs of images with the 1-pixel shift and 2-pixel shift, they were considered the same in 80.7% and 56.0% of the responses, respectively. As expected, the shifts become easier to detect as the size of the shifts increases. But even for pairs of the 5-pixel shift, they were still not identified in 26.7% of the responses. As shown in our study, even after being informed about the possible shifts, participants still had difficulty in detecting small shifts. This verifies our hypothesis that it is difficult for people to detect a small shift in images.

4 Effect of Small Shifts on Similarity Metrics

To understand how existing similarity metrics handle small shifts between a pair of images, we benchmarked representative metrics, including off-the-shelf metrics, such as L2 and SSIM, and recent deep learning-based metrics. We derived a new dataset from the Berkeley-Adobe Perceptual Patch Similarity Dataset (BAPPS) (Zhang et al., 2018) in our study. The original BAPPS dataset consists of 36,344 examples, each with a reference image I_r, and two distorted images I_1 and I_2. These samples cover a wide range of common distortions, including traditional, CNN-based, and from real-algorithms such as superresolution, frame interpolation, deblurring, and colorization. Please refer to Zhang et al. (2018) for more details. For each sample in the BAPPS dataset, we shifted the distorted images horizontally by k pixels where $k \in \{1, 2, 3\}$. To avoid any boundary artifacts from shifting, we cropped each shifted image I_i as follows.

$$\hat{I}_i = I_i[\,0 : h,\ k : (w + k - 3)] \tag{1}$$

where w and h are the original image size. In this way, all the images in our test were of size $(w - 3) \times h$ without regard to the amount of shift, which eliminates the effect of image sizes when we test how the amount of shift affects the performance of metrics. The reference images were also cropped to the same size as the distorted images but no shifts were applied. In addition, we also cropped all the images in each original sample to the size of $(w-3) \times h$ in order to make the shifted sample and the original sample the same size to avoid the effect of the image size on a similarity metric in our late experiments. No shift was introduced to the original samples.

When evaluating a similarity metric, we applied it to both the original sample in the BAPPS dataset as well as its corresponding shifted once. Specifically, for each sample, we obtained two pairs of similarity scores, (s_1, s_2) and $\hat{s}_1, \hat{s}_2$. (s_1, s_2) are the similarity scores between I_1 and its reference image I_r, and I_2 and I_r, respectively. $(\hat{s}_1, \hat{s}_2)$ are the corresponding pair of similarity scores for the shifted sample. Each pair of scores indicates which of the two distorted images is more similar to the reference image according to the metric used in the test. We count the number of samples for which the similarity rank flips when a sample was shifted and compute the rank-flip rate as follows.

$$r_{rf} = \frac{1}{N} \sum_{l=1}^{N} (s_1^l < s_2^l) \neq (\hat{s}_1^l < \hat{s}_2^l) \tag{2}$$

where r_{rf} is the rank-flip rate and N is the number of samples in the test set. We use r_{rf} to evaluate how robust a metric is against the small shift between a pair of images.

For all the learned metrics involved in this study, we used the trained models shared by their authors unless otherwise noted. While the image size of the BAPPS dataset is 256×256, some models shared by their authors were trained on 64×64 resized images. Therefore we conducted studies on these two sizes separately to provide fair and informative comparisons.

Table 1: Accuracy (2AFC) & shift-tolerance (r_{rf}) of various metrics on the BAPPS validation dataset. 2AFC is computed on the BAPPS dataset resized 64×64 while r_{rf} scores are obtained from its shifted version of size 64×61.

Network	2AFC	r_{rf}		
		1 pixel	2 pixel	3 pixel
L2	62.91	12.27	23.07	28.83
SSIM Wang et al. (2004)	63.08	13.08	25.50	32.74
E-LPIPS Kettunen et al. (2019)	69.23	8.72	10.67	12.34
GTI-CNN Ma et al. (2018)	63.74	9.37	12.32	16.25
DISTS Ding et al. (2020)	68.89	5.57	8.20	10.07
PIM-1 Bhardwaj et al. (2020)	69.45	**1.63**	**3.06**	**4.39**
PIM-5 Bhardwaj et al. (2020)	69.47	2.28	3.56	5.19
LPIPS (Alex) Zhang et al. (2018)	69.83	6.79	8.90	9.70
LPIPS (Alex) retrained from scratch*†	**70.04**	9.25	9.34	11.55
LPIPS (Alex) ours*†	69.83	3.48	4.75	6.84

$*$ Trained on image patches of size 64 using author's (†) setup.

Table 2: Accuracy (2AFC) & shift-tolerance (r_{rf}) across various metrics on the BAPPS validation dataset. 2AFC is computed on the BAPPS dataset of original size 256×256 while r_{rf} is obtained from its shifted version of size 256×253.

Network	2AFC	r_{rf}		
		1 pixel	2 pixel	3 pixel
L2	62.92	3.59	7.55	10.82
SSIM (Wang et al., 2004)	61.41	3.16	7.20	13.73
MS-SSIM (Wang et al., 2003)	62.54	2.22	5.83	10.66
PIEAPP Sparse (Prashnani et al., 2018)	64.20	2.83	3.19	3.81
PIEAPP Dense (Prashnani et al., 2018)	64.15	2.97	1.37	3.33
PIM-1 (Bhardwaj et al., 2020)	67.45	0.79	1.70	2.52
PIM-5 (Bhardwaj et al., 2020)	67.38	1.01	1.88	2.96
GTI-CNN (Ma et al., 2018)	63.87	3.95	4.91	7.88
DISTS (Ding et al., 2020)	68.83	2.85	2.89	4.03
E-LPIPS (Kettunen et al., 2019)	68.22	5.84	5.86	5.77
LPIPS (Alex) (Zhang et al., 2018)	68.59	2.81	3.41	3.84
LPIPS (Alex) retrained from scratch*†	70.54	2.58	3.59	3.53
LPIPS (Alex) ours*†	70.39	0.66	1.24	1.79
LPIPS (Alex) retrained from scratch*‡	**70.65**	2.87	3.92	3.74
LPIPS (Alex) ours*‡	70.48	**0.57**	**1.06**	**1.50**

$*$ Trained on patches of size 256 using author's (†) / our (‡) setup.

We report the results in Table 1 and Table 2. All scores are obtained by averaging over examples in each distortion category in the BAPPS dataset and then averaging over all the categories. The two-alternative forced choice (2AFC) scores were obtained from the original BAPPS dataset that indicates how a metric's prediction correlates with the human opinion (Zhang et al., 2018). The rank-flip rate (r_{rf}) is calculated from the shifted dataset. It shows how robust a metric is to the shift between a distorted image and its reference image. As reported in Table 2, the learned metrics match the human perception better than the non-learned ones such as L2, SSIM, and MS-SSIM. However, even these learned metrics are sensitive to small shifts except for the recent metric, PIM (Bhardwaj et al., 2020). Compared to these existing metrics except PIM, our metrics are more consistent with human perception as per 2AFC scores and more robust against small shifts. Overall, our method is comparable to PIM. Our method outperforms PIM on images of size 256×256 (Table 2) but does not work as well as it on smaller images (Table 1). As discussed in Section 2, PIM is trained from neighboring video frames which often contain small shifts, which makes it robust against the imperceptible shifts. Our work is orthogonal to PIM in that we investigate neural network elements to build a robust similarity metric. Therefore, we purposely trained our metrics on the BAPPS dataset without any data augmentation.

5 Elements of Shift-tolerant Metrics

Some recent papers reported that training a deep neural network using samples with shifted images through either data augmentation or neighboring video frames can make a learned similarity metric robust against small shifts between a pair of images (Ma et al., 2018; Bhardwaj et al., 2020). This paper aims to solve this problem from a different perspective; we investigate how one can design a deep neural network that can be resistant to small shifts. We select the LPIPS network architecture as our baseline framework as it correlates with the human visual similarity judgment well (Zhang et al., 2018). To make this paper self-complete, we briefly describe the LPIPS framework. As illustrated in Figure 3, LPIPS first uses a backbone network, such as AlexNet (Krizhevsky et al., 2012) and VGG (Simonyan & Zisserman, 2015), to extract multi-level feature embeddings from a distorted image I_{dst} or its reference image I_{ref}. We denote the resulting feature embeddings as F_{dst} and F_{ref}, respectively. It then calcu-

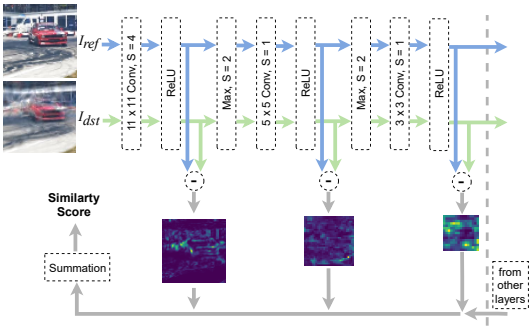

Figure 3: LPIPS framework. The same feature extraction network (AlexNet) is used to extract feature embeddings from I_{dst} and I_{ref}. The difference between these embeddings is calculated at different levels and is combined together as the similarity between I_{dst} and I_{ref}.

lates the difference between F_{dst} and F_{ref} at all the levels and linearly combines the embedding difference at different levels into a final similarity / difference score, denoted as $d(F_{dst}, F_{ref})$. The combination coefficients and the feature extraction network are learned or fine-tuned.

Below we discuss how various neural network elements affect a similarity metric and how they can be improved to handle imperceptible shifts between a pair of images. Our focus is to develop a feature extraction network to generate feature embeddings from a pair of images that 1) are invariant to imperceptible shifts and 2) lead to a metric that correlates well with the human judgements.

Reducing Stride. Striding is widely used in a deep neural network to reduce the input size. For instance, AlexNet has a strided convolution (stride=4) in its first convolutional layer (*conv-1*) and many max pooling operators with stride=2 in the rest of the network. However, it is commonly known that striding with size >1 leads to the sampling rate falling well below the Nyquist rate, which causes aliasing artifacts. In their experiments with image classification tasks, Azulay & Weiss (2019) showed that AlexNet without any subsampling is significantly less sensitive to translations and also maintains its accuracy. Similarly, we also investigate the reduction of the stride size in the convolutional layers in the LPIPS framework to make it more resistant to imperceptible shifts at no expense of its consistency with the human visual similarity perception.

Anti-aliasing. Convolution is the most common operator for a deep convolutional neural network. A pure convolutional operator is shift-equivariant instead of being shift-invariant (Nair & Hinton, 2010). Shift equivariance makes a learned similarity metric sensitive to small shifts as small shifts between two images I_{dst} and I_{ref} will be transferred to the shifts between their feature embeddings F_{dst} and F_{ref}, which will in term drastically increase the distance between the feature embeddings $d(F_{dst}, F_{ref})$ as shown in Figure 4 (b). Downsampling in a neural network improves its shift invariance. Typically, downsampling can be achieved by a strided convolutional operator or a strided pooling operator with stride n ($n > 1$). However, as discussed earlier in Reducing Stride, striding introduces aliasing. While reducing stride size lessens aliasing, it prevents the network from reducing the feature size.

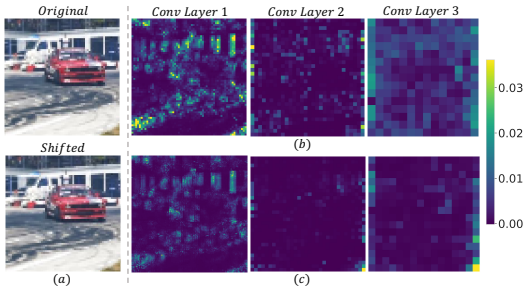

Figure 4: Feature embedding difference maps at different levels. (a) an input image and its one-pixel shifted version. (b) difference maps between embeddings extracted by the original AlexNet. (c) difference maps between embeddings extracted by AlexNet augmented with anti-aliased strided convolution and pooling layers.

To keep the benefit of downsampling while reducing stride, Zhang (2019) invented a *BlurPool* operator. Take max pooling with stride n as an example. Such a max pooling operator can be decomposed into two steps: max pooling with stride 1, followed by a downsampling operator with stride n. To reduce the aliasing artifacts, Zhang (2019) followed the pre-filtering idea for anti-aliasing and replaced this max pooling operator with a sequence of three operators: a max pooling with stride 1, a Gaussian filter, and a downsampling operator with stride n. The last two operators are combined into as a single operator, called *BlurPool*. Similarly, a convolution operator with stride n can be replaced with its anti-aliased version as a convolution operator with stride b and *BlurPool* with stride n/b. Zhang (2019) found that replacing the original convolutional and pooling layers in a feature extraction neural network with their *BlurPool* versions helps generate feature embeddings that make the downstreaming tasks more shift invariant. *BlurPool* uses a fixed Gaussian filter for blurring and may lose some spatial features that are important attributes defining the quality of an image. Zou et al. (2020) developed an adaptive anti-aliasing filter by learning a low-pass filter that is more content-aware. In this paper, we replace the strided convolution layers or pooling layers in the LPIPS framework with *BlurPool* or adaptive anti-aliasing filters to make it invariant to imperceptible shifts among images in a pair. Figure 4 (c) shows that while anti-aliased convolution and pooling layers cannot make the feature network completely shift-invariant, they significantly reduce the difference between the feature embeddings from a pair of shifted images.

Location of Anti-aliasing. In a deep neural network, such as AlexNet used in LPIPS, a convolution layer is usually followed by an activation function like *ReLU*. According to Zhang (2019), the activation function is inserted between the stride-reduced convolutional layer and *BlurPool*, as illustrated

in Figure 5 (a). Vasconcelos et al. (2021) created variants of the anti-aliased strided convolution by placing the anti-aliasing filter at different locations, specifically, before or after the convolution operation. They found that some variants can lead to stronger learned inductive priors. But, will they provide significant improvements in shift tolerance? We build upon their findings and design variations of the anti-aliased strided convolutions. Specifically, we modify AlexNet *conv-1* as illustrated in Figure 5 and explain the variants below.

Original. As shown in Figure 5 (a), we follow the original design of *BlurPool* and put it after *ReLU* (Zhang, 2019). For anti-aliasing, the stride size of *conv-1* is reduced from 4 to 2 and the *BlurPool* layer has a stride of 2 so that the total stride of 4 is preserved in this anti-aliased version. We take the output of *ReLU* as the feature embedding to calculate the similarity.

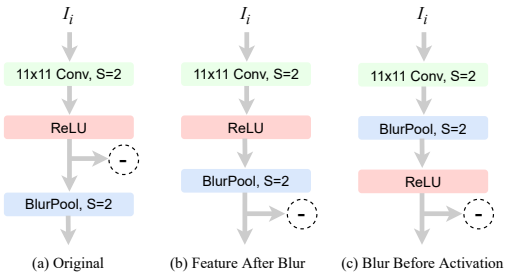

Figure 5: Alternative positions of *BlurPool*.

Feature after blur. In the above design, the feature embedding is used before *BlurPool*. This effectively reduces the anti-aliasing effect on the feature embeddings although the reduced stride size in *conv-1* still offers some level of anti-aliasing. Therefore, we investigated a variation of the anti-aliased convolution by taking the output of *BlurPool* as the feature embedding to be used for similarity calculation, as illustrated in Figure 5 (b).

Blur before activation. Vasconcelos et al. (2021) suggested that blurring after the non-linearity, as done in Figure 5 (a) and (b), prevents high frequency from getting passed on to subsequent layers. Following their findings, we adopted their design by placing *BlurPool* before *ReLU* to keep the high-frequency information from *ReLU*, as shown in Figure 5 (c).

Border Handling. Islam et al. (2020) reported that feature embeddings extracted by a convolutional neural network encode absolute position information. This has an important implication for a learning-based similarity metric that feature embeddings from a convolutional neural network are position-dependent and are not shift-invariant. They found that zero padding can relieve this boundary problem for computer vision tasks that are sensitive to spatial information. Kayhan & Gemert (2020) further proposed the concept of full convolution (F-Conv), in which every element of the filter needs to be applied to every pixel in the input image. They implemented F-Conv as a regular convolutional operator with zero padding of $2k$ where $2k+1$ is the filter kernel size, as illustrated in Figure 7 (Appendix A.2). Note, F-Conv will make the output of an un-strided convolution operator $2k$ larger than the input. They reported that F-Conv is least sensitive to the absolute position of the objects for image classification tasks. Inspired by these works, we replace the regular convolution operators with F-Conv in the LPIPS framework and increase the padding size in *BlurPool* operators to achieve better shift-invariance.

Pooling. Max pooling is well known for being more shift invariant than average pooling. We investigate whether its anti-aliased version, *MaxBlurPool* (described earlier in Anti-aliasing) is also more shift invariant than *AvgBlurPool*, the anti-aliased version of average pooling when used in the LPIPS framework. Average pooling in its original form already supports anti-aliasing. We follow Zhang (2019) and implement *AvgBlurPool* with a stride of n as Gaussian filtering followed by downsampling with a factor of n.

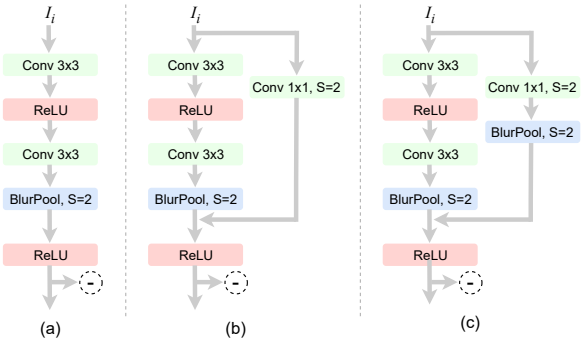

Figure 6: Anti-aliased skipped connection. (a) VGG-like network with AvgBlurPool, (b) with skip connection, and (c) with anti-aliased skip connection.

Strided-skip Connections. Skip connection is widely used in a deep neural network to speedup training and obtain a high quality neural network model. We investigate whether skip connection helps improve shift invariance of a learned similarity metric. As discussed in Vasconcelos et al. (2021), a strided skip connection introduces aliasing for the same reason discussed earlier in Anti-aliasing. We therefore explore anti-aliased strided skip connections, as shown in Figure 6.

6 EXPERIMENTS

We built upon the LPIPS framework and incorporated the elements discussed in Section 5 to investigate how these elements help develop a similarity metric that is consistent with the human visual similarity judgement and is robust against imperceptible shifts. We first compare our metrics to both off-the-shelf metrics, such as SSIM and MS-SSIM, and the recent learned similarity metrics. We then conduct ablation studies to evaluate how these elements work.

Comparisons to Existing Metrics. In Section 4, we derived a shifted dataset from the BAPPS dataset and compared our metrics to representative existing metrics (Bhardwaj et al., 2020; Ding et al., 2020; Ma et al., 2018; Kettunen et al., 2019; Prashnani et al., 2018; Wang et al., 2004; 2003; Zhang et al., 2018). In our experiments, we adopt the 2AFC metric to evaluate how consistent a metric is with human judgment, and the rank-flipping rate, r_{rf}, to evaluate how robust it is against small shifts. As shown in Table 1 and 2, our metrics are both more consistent with human visual similarity judgment and more robust against imperceptible shifts than most of them, except a recent metric PIM (Bhardwaj et al., 2020), to which our method is comparable. PIM achieves shift robustness by training on neighboring video frames that often have small shifts. We work on an orthogonal solution by investigating neural network elements to make the learned metric robust and therefore only train our metrics on the examples without any shift through data augmentation. We further evaluated the metrics on the perceptual validation dataset from the 2021 Challenge on Learned Image Compression (CLIC). The results in Table 3 are consistent with previous results, i.e., our method outperforms all the other methods in terms of accuracy and is more shift-robust than others except PIM, which is similarly robust to ours.

Table 3: Experiments on the CLIC dataset.

Network	Accuracy(%)	Number of rank flips		
		1 pix	2 pix	3 pix
L2	58.16	833	2102	2214
SSIM (Wang et al., 2004)	60.00	349	931	1109
PIEAPP (Prashnani et al., 2018)	75.44	91	134	158
E-LPIPS[12]	74.44	212	251	317
DISTS (Ding et al., 2020)	75.63	28	36	50
PIM-1 (Bhardwaj et al., 2020)	73.79	**13**	22	33
LPIPS(Alex) (Zhang et al., 2018)	73.68	90	108	121
LPIPS(Alex) retrained from scratch*†	76.53	59	51	62
LPIPS(Alex) ours*†	**76.97**	17	**14**	**21**

$*$ Trained on image patches of size 64 using author's (†) setup.

Ablation Studies. We now examine how individual network elements affect our metrics. In these studies, we trained all our metrics using the original BAPPS training set on their original size of 256×256. We purposely did not train on the shifted version to focus on neural network element designs. To train our metrics, we used the loss function: $MSE(s, h)$, where $s = s_1/(s_1 + s_2)$, s_1 and s_2 are the predicted similarity scores of two images I_1 and I_2 to their corresponding reference image, and h is the human score. We trained our metrics using the same settings as Zhang et al. (2018) except we used a lower dropout rate of 0.01. We tested all our metrics on the shifted testing dataset to obtain the rank-flipping rate. To obtain the 2AFC scores, we ran our metrics on the full-size images (with no shift) of the original BAPPS dataset so that we could verify whether our metrics sacrifice consistency with human visual similarity judgment to be robust against imperceptible shifts.

We first examine elements discussed in Section 5 individually. We use AlexNet as the backbone feature extraction network with the LPIPS framework as it provides the best result among other backbone networks (Zhang et al., 2018). As reported in Table 4, anti-aliasing via *BlurPool* can greatly improve LPIPS's robustness against imperceptible shifts. Reducing stride size in its strided convolutional layer (*conv-1*) also helps making it significantly more robust at little expense of the 2AFC score. Combining *BlurPool* with reducing stride size makes the network even more robust against imperceptible shifts and more consistent with human judgment based on the 2AFC score. Then a larger reflection padding size also helps as it reduces the position information encoded in the feature embeddings from the image boundaries, as discussed in Section 5. However, F-Conv, also designed to reduce the boundary issue, does not help. While the learned *BlurPool* (Zou et al., 2020) also helps, it is not as effective as the original version for our task of making a robust similarity metric.

Table 4: Effect of (1) anti-aliasing (AA) via *BlurPool*, (2) F-Conv, (3) reduced stride, & (4) adaptive-AA§ on learned metrics.

AA (BlurPool) Reflection-Pad 1	AA (BlurPool) Reflection-Pad 2	F-Conv	Stride in *conv-1*	2AFC	r_{rf} 1 pixel	r_{rf} 2 pixel	r_{rf} 3 pixel
			4	70.65	2.87	3.92	3.74
✓			2	70.53	1.85	2.22	2.58
	✓		2	**70.67**	1.46	1.82	2.25
		✓	4	70.57	2.78	3.92	3.91
	✓	✓	2	70.52	1.77	2.15	2.48
			2	70.54	1.84	2.28	2.34
	✓		1	70.42	0.66	**1.13**	1.83
	✓	✓	1	70.44	**0.63**	1.14	**1.68**
✓§			2	70.57	2.63	3.36	3.16
	✓§		2	70.63	2.80	3.57	3.39
	✓§	✓	2	70.52	2.95	4.13	3.93

§ (Zou et al., 2020)

We test on different backbone feature networks, including VGG-16 (Simonyan & Zisserman, 2015), ResNet-18 (He et al., 2016), and SqueezeNet (Iandola et al., 2016). While reducing the stride size is effective, not all networks have a strided convolution layer. Hence, we focus on *BlurPool* applied to pooling layers. As shown in Table 5, *BlurPool* significantly improves the robustness of other backbone networks as well. What is interesting is the effect of the padding size within these backbone networks. While a larger padding size improves 2AFC scores, it does not make shift-invariance better for VGG-16 and ResNet-18. For them, the anti-aliased convolution layers have a stride size of 1, which leads to minor boundary issues. We conjecture that this makes a larger padding size unnecessary.

Table 5: Anti-aliasing via *BlurPool* can significantly improve shift-tolerance and often improve 2AFC scores consistently for different backbone feature extraction networks.

Network	AA (BlurPool)		2AFC	r_{rf}		
	Reflection-Pad					
	1	2		1 pixel	2 pixel	3 pixel
VGG-16			70.03	3.01	3.76	3.44
	✓		70.05	**0.66**	**1.08**	**1.44**
		✓	**70.07**	**0.66**	1.12	1.82
ResNet-18			69.86	2.67	3.35	3.77
	✓		69.95	**0.82**	**1.51**	**2.19**
		✓	**70.14**	1.07	1.81	2.38
Squeeze			69.61	7.41	7.58	10.35
	✓		69.24	**2.03**	3.06	3.93
		✓	**69.44**	2.10	**2.48**	**3.42**

We also examine the effect of the location of *BlurPool* within AlexNet. As reported in Table 6, the original version (Figure 5 (a)) works best when the stride size is 2 in *conv-1*. With a smaller stride size, it does not work as well as Blur Before Activation (Figure 5 (c)). This is in part consistent with what was found by Vasconcelos et al. (2021). In the original design, *BlurPool* is placed after the activation layer for anti-aliasing at the expense of the reduction of the high-frequency information from the activation layer. With the need for anti-aliasing due to a larger stride size, this trade-off works out. However, when stride size is 1, the need for anti-aliasing is reduced; therefore, it is more helpful to place *BlurPool* before the activation layer to avoid the loss of high-frequency information. Thus, Blur Before Activation works better when the stride size is 1.

Table 6: Effect of *BlurPool* locations within an anti-aliased strided convolution as illustrated in Figure 5.

Anti-Alias (BlurPool)	Stride in *Conv-1*	BlurPool Location	2AFC	r_{rf}		
				1 pixel	2 pixel	3 pixel
✓	2	Original	**70.67**	**1.46**	**1.82**	**2.25**
✓	2	FeatureAfterBlur	70.55	1.73	1.84	2.49
✓	2	BlurBeforeActivation	70.50	2.06	2.02	2.74
✓	1	Original	70.42	0.66	1.13	1.83
✓	1	FeatureAfterBlur	**70.52**	0.69	1.11	1.60
✓	1	BlurBeforeActivation	70.48	**0.57**	**1.06**	**1.50**

Table 7 shows that *MaxBlurPool* has better shift tolerance but lower 2AFC scores (accuracy) than *AvgBlurBool*. Moreover, using anti-aliased strided-skip connections leads to higher accuracy with a negligible drop in shift tolerance.

Table 7: Effects of different pooling layers and anti-aliased strided skip connections.

Network elements	2AFC	r_{rf}		
		1 pixel	2 pixel	3 pixel
AvgBlurPool	69.88	1.24	1.86	2.18
MaxBlurPool	69.58	0.95	1.54	2.12
AvgBlurPool & Strided Skip	69.82	1.38	2.06	2.61
AvgBlurPool & Anti-aliased Skip	70.05	1.26	1.89	2.32
MaxBlurPool & Anti-aliased Skip	69.86	1.07	1.66	2.35

Summary. Among the network elements we investigated, anti-aliased strided convolution, anti-aliased pooling, and reduction of stride size are most effective to develop a perceptual similarity metric that is robust against imperceptible shifts. These findings are consistent across a variety of backbone network architectures. A larger padding size helps reduce the position information due to the boundary issues encoded in the feature embeddings. Anti-aliased skip connection can help improve accuracy but with little effect on shift invariance. The position of *BlurPool* matters. It should be placed before the activation layer if its precedent convolution uses a small stride size.

7 Conclusion

This paper reported our investigation on how to design a deep neural network as a learned perceptual image similarity metric that is both consistent with the human visual similarity judgement and robust against the imperceptible shift among a pair of images. We discussed various neural network elements, such as anti-aliased strided convolution, anti-aliased pooling, the placement of *BlurPool*, stride size, and skip connection and studied their effect on a similarity metric. We found that using anti-aliasing strided convolutions and pooling operators and reducing stride size are very helpful to make a learned similarity metric shift-invariant. Our experiments show that by integrating these elements into a neural network, we are able to develop a learned metric that is more robust against imperceptible shifts and more consistent with the human visual similarity judgement.

REFERENCES

Anish Athalye, Nicholas Carlini, and David Wagner. Obfuscated gradients give a false sense of security: Circumventing defenses to adversarial examples. In *International Conference on Machine Learning*, volume 80, pp. 274–283, 2018.

Aharon Azulay and Yair Weiss. Why do deep convolutional networks generalize so poorly to small image transformations? *Journal of Machine Learning Research*, 20(184):1–25, 2019.

Sangnie Bhardwaj, Ian Fischer, Johannes Ballé, and Troy Chinen. An unsupervised information-theoretic perceptual quality metric. In *Advances in Neural Information Processing Systems*, pp. 13–24, 2020.

Steffen Czolbe, Oswin Krause, Ingemar Cox, and Christian Igel. A loss function for generative neural networks based on watson's perceptual model. In *Advances in Neural Information Processing Systems*, pp. 2051–2061, 2020.

Keyan Ding, Kede Ma, Shiqi Wang, and Eero P. Simoncelli. Image quality assessment: Unifying structure and texture similarity. *IEEE Transactions on Pattern Analysis and Machine Intelligence*, pp. 1–1, 2020.

Alexey Dosovitskiy and Thomas Brox. Generating images with perceptual similarity metrics based on deep networks. In *Advances in Neural Information Processing Systems*, pp. 658–666, 2016.

Jinjin Gu, Haoming Cai, Haoyu Chen, Xiaoxing Ye, Jimmy S. Ren, and Chao Dong. Pipal: A large-scale image quality assessment dataset for perceptual image restoration. In *European Conference on Computer Vision*, volume 12356, pp. 633–651, 2020.

Kaiming He, Xiangyu Zhang, Shaoqing Ren, and Jian Sun. Deep residual learning for image recognition. In *IEEE Conference on Computer Vision and Pattern Recognition*, pp. 770–778, 2016.

Olivier J Hénaff and Eero P Simoncelli. Geodesics of learned representations. In *International Conference on Learning Representations*, 2016.

Forrest N. Iandola, Song Han, Matthew W. Moskewicz, Khalid Ashraf, William J. Dally, and Kurt Keutzer. Squeezenet: Alexnet-level accuracy with 50x fewer parameters and <0.5mb model size. *arXiv preprint arXiv:1602.07360*, 2016.

Md Amirul Islam, Sen Jia, and Neil D. B. Bruce. How much position information do convolutional neural networks encode? In *International Conference on Learning Representations*, 2020.

Justin Johnson, Alexandre Alahi, and Li Fei-Fei. Perceptual losses for real-time style transfer and super-resolution. In *European Conference on Computer Vision*, volume 9906, pp. 694–711, 2016.

Osman Semih Kayhan and Jan C. van Gemert. On translation invariance in cnns: Convolutional layers can exploit absolute spatial location. In *Proceedings of the IEEE Conference on Computer Vision and Pattern Recognition*, pp. 14262–14273, 2020.

Markus Kettunen, Erik Härkönen, and Jaakko Lehtinen. E-LPIPS: Robust perceptual image similarity via random transformation ensembles. *arXiv preprint arXiv:1906.03973*, 2019.

Diederik P Kingma and Max Welling. Auto-encoding variational bayes. In *International Conference on Learning Representations*, 2013.

Alex Krizhevsky, Ilya Sutskever, and Geoffrey E. Hinton. ImageNet classification with deep convolutional neural networks. In *Advances in Neural Information Processing Systems*, pp. 1106–1114, 2012.

Christian Ledig, Lucas Theis, Ferenc Huszar, Jose Caballero, Andrew P. Aitken, Alykhan Tejani, Johannes Totz, Zehan Wang, and Wenzhe Shi. Photo-realistic single image super-resolution using a generative adversarial network. *arXiv/1609.04802*, 2016.

Jake Lee, Junfeng Yang, and Zhangyang Wang. What does cnn shift invariance look like? a visualization study. In *European Conference on Computer Vision – Workshops*, pp. 196–210. Springer, 2020.

Tsung-Yi Lin, Michael Maire, Serge Belongie, James Hays, Pietro Perona, Deva Ramanan, Piotr Dollár, and C Lawrence Zitnick. Microsoft coco: Common objects in context. In *European conference on computer vision*, pp. 740–755. Springer, 2014.

Kede Ma, Zhengfang Duanmu, and Zhou Wang. Geometric transformation invariant image quality assessment using convolutional neural networks. In *2018 IEEE International Conference on Acoustics, Speech and Signal Processing (ICASSP)*, pp. 6732–6736, 2018.

Douglas L Medin, Robert L Goldstone, and Dedre Gentner. Respects for similarity. *Psychological review*, 100(2):254, 1993.

Vinod Nair and Geoffrey E Hinton. Rectified linear units improve restricted boltzmann machines. In *International Conference on Machine Learning*, pp. 807–814, 2010.

Simon Niklaus, Long Mai, and Feng Liu. Video frame interpolation via adaptive separable convolution. In *Proceedings of the IEEE International Conference on Computer Vision*, pp. 261–270, 2017.

Ekta Prashnani, Hong Cai, Yasamin Mostofi, and Pradeep Sen. Pieapp: Perceptual image-error assessment through pairwise preference. In *Proceedings of the IEEE Conference on Computer Vision and Pattern Recognition*, pp. 1808–1817, 2018.

Mehdi S. M. Sajjadi, Bernhard Schölkopf, and Michael Hirsch. EnhanceNet: Single image super-resolution through automated texture synthesis. *arXiv/1612.07919*, 2016.

Karen Simonyan and Andrew Zisserman. Very deep convolutional networks for large-scale image recognition. In *International Conference on Learning Representations*, 2015.

Amos Tversky. Features of similarity. *Psychological review*, 84(4):327, 1977.

Cristina Vasconcelos, Hugo Larochelle, Vincent Dumoulin, Rob Romijnders, Nicolas Le Roux, and Ross Goroshin. Impact of aliasing on generalization in deep convolutional networks. In *IEEE International Conference on Computer Vision*, 2021.

Zhou Wang, Eero P Simoncelli, and Alan C Bovik. Multiscale structural similarity for image quality assessment. In *The Thrity-Seventh Asilomar Conference on Signals, Systems & Computers*, volume 2, pp. 1398–1402. IEEE, 2003.

Zhou Wang, Alan C Bovik, Hamid R Sheikh, and Eero P Simoncelli. Image quality assessment: from error visibility to structural similarity. *IEEE transactions on image processing*, 13(4):600–612, 2004.

Andrew B Watson. DCT quantization matrices visually optimized for individual images. In *Human vision, visual processing, and digital display IV*, volume 1913, pp. 202–216. International Society for Optics and Photonics, 1993.

Chaowei Xiao, Jun-Yan Zhu, Bo Li, Warren He, Mingyan Liu, and Dawn Song. Spatially transformed adversarial examples. In *International Conference on Learning Representations*, 2018.

Lin Zhang, Lei Zhang, Xuanqin Mou, and David Zhang. Fsim: A feature similarity index for image quality assessment. *IEEE transactions on Image Processing*, 20(8):2378–2386, 2011.

Richard Zhang. Making convolutional networks shift-invariant again. In *International Conference on Machine Learning*, pp. 7324–7334, 2019.

Richard Zhang, Phillip Isola, Alexei A Efros, Eli Shechtman, and Oliver Wang. The unreasonable effectiveness of deep features as a perceptual metric. In *Proceedings of the IEEE Conference on Computer Vision and Pattern Recognition*, pp. 586–595, 2018.

Jun-Yan Zhu, Philipp Krähenbühl, Eli Shechtman, and Alexei A. Efros. Generative visual manipulation on the natural image manifold. In *European Conference on Computer Vision*, volume 9909, pp. 597–613, 2016.

Xueyan Zou, Fanyi Xiao, Zhiding Yu, and Yong Jae Lee. Delving deeper into anti-aliasing in convnets. In *The British Machine Vision Conference (BMVC)*, 2020.

A APPENDIX

A.1 USER STUDY

We recruited 32 participants for our study. These participants have a wide range of professional background, including computer science, business, medicine, arts and education. Most of them are between 20 to 35 years old.

To ensure the quality of this user study, we removed the responses from two participants who failed to pass a validation test. Specifically, if a participant identified a pair of images with 0-pixel shift as *different* or a pair of images with 9-pixel shift as *the same* for more than two-thirds of the time in the study, we did not include the response from that participant. In total, 30 participants passed our validation test. We in total obtained responses to 1500 trials, with 150 responses for each of the n-pixel shifts.

It is important to disclose that before the study, we informed our participants that there might be shifts between some pairs of images in order to raise their alert to the potential difference created by shift. While this might bias participants, we found it helpful to obtain more informative understanding on human perception of small shifts; otherwise participants tended to overly overlook the difference between a pair of images.

A.2 FULL CONVOLUTION

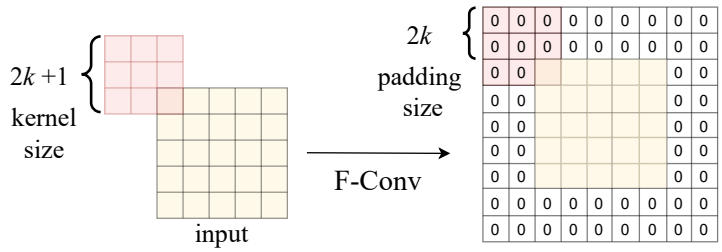

Figure 7: Illustration of Full Convolution (F-Conv), where every value of the filter needs to be applied to each value of an input image. Hence, the input needs to be padded first with padding size $2k$ for a filter with size $2k + 1$ Kayhan & Gemert (2020).

A.3 ADDITIONAL ABLATION STUDIES

We provide a few additional ablation studies to help examine the network elements discussed in our main paper.

A.3.1 PADDING SIZE

Table 8: Effects of increasing reflection-pad size. This test is conducted for our learned metric using AlexNet as its backbone network.

AA (*BlurPool*) w/ Reflection-Pad	2AFC	r_{rf} 1 pixel	r_{rf} 2 pixel	r_{rf} 3 pixel
None	70.53	2.11	2.51	2.58
1	70.53	1.85	2.22	2.58
2	70.67	1.46	1.82	2.25

To further examine the effect of the padding size, we added a new variation where no padding is used in all the *BlurBool* layers. As shown in Table 8, padding in the *BlurPool* layers makes our learned metric more robust against small shifts.

A.3.2 BLUR KERNEL SIZE

Table 9: Effects of increasing the blur kernel size.

AA (*BlurPool*) Reflection-Pad		Stride	Blue Kernel Size	2AFC	r_{rf}		
1	2	*in Conv-1*	*in Conv-1*		1 pixel	2 pixel	3 pixel
✓		2	3	70.53	1.85	2.22	2.58
✓		2	5	70.60	1.57	1.67	2.21
	✓	2	3	70.67	1.46	1.82	2.25
	✓	2	5	70.54	1.61	1.55	2.16
	✓	1	3	70.42	0.66	1.13	1.83
	✓	1	5	70.57	0.73	1.16	1.71

BlurPool is used for anti-aliasing for strided convolution and strided pooling operators Zhang (2019). Anti-aliasing is achieved by employing a Gaussian filter to remove the high-frequency in the intermediate result from its previous step of non-striding pooling or convolution operators. A key parameter is the size of Gaussian filter kernel. In our paper, we used a fixed kernel size of 3. We add a new test to examine the effect of the kernel size in *conv-1* on our learned metric. As shown in the first group of Table 9, a large kernel helps anti-aliasing in general and thus makes our metric more shift-tolerant. However, when combined with a reduced stride size (=1), a large kernel can also be counter productive and make our metric less shift-invariant, as shown in the bottom group in Table 9. This is because when the stride size is 1, aliasing is not a big issue. Then a large kernel size removes useful high-frequency information with little gain from anti-aliasing.

A.3.3 PADDING TYPE

Table 10: Comparing the type of padding, Zero vs. Reflection, in the BlurPool layers.

AA (*BlurPool*)				r_{rf}		
Refl-Pad Size 2	Zero-Pad Size 2	F-Conv	2AFC	1 pixel shift	2 pixel shift	3 pixel shift
✓			70.67	**1.46**	**1.82**	**2.25**
	✓		70.55	2.05	2.28	2.70
✓		✓	70.52	1.77	2.15	2.48
	✓	✓	**70.72**	1.80	2.24	2.40

In all our experiments, we set the default padding type as reflection padding. We now examine if zero padding performs better or not by replacing reflection padding with zero padding in the *BlurPool* layers. As shown in Table 11, we found that reflection padding in general outperforms zero padding.

A.3.4 ANTI-ALIASING OPERATOR TYPE

Table 11: Comparing BlurPool against l_2 pooling.

Anti-alias		Blur Kernel Size	2AFC	r_{rf}		
BlurPool	l_2 Pooling	in all layers		1 pix	2 pix	3 pix
✓		3	70.53	1.85	2.22	2.58
	✓	3	70.69	2.92	3.90	3.60
✓		5	70.51	1.68	1.59	2.17
	✓	5	70.55	1.87	1.89	2.38

We use BlurPool for anti-aliasing in all our experiments. Here we compare the effect of anti-aliasing via *BlurPool* versus l_2 *Pooling*. When the blur kernel size is 3, the shift tolerance of the network having *BlurPool* is substantially better than the network with l_2 *Pooling* layers, but at the expense of accuracy. This maybe due to a weaker blurring by l_2 *Pooling*. As the blur kernel size is increased to 5, the strength of the blurring effect increases in both, and we observe the performance gap reducing, in terms of both accuracy and shift tolerance.